PHYSICAL REVIEW B VOLUME 24, NUMBER 4 15 AUGUST 1981

Bulk-energy-band structure of TiN: An angle-resolved-photoemission study of the (100) surface

L. I. Johansson and A. Callenås
Department of Physics and Measurement Technology, Linköping University, S-581 83 Linköping, Sweden

P. M. Stefan
Stanford Electronics Laboratories, Stanford University, Stanford, California 94305

A. Nørlund Christensen
Department of Chemistry, Aarhus University, DK-8000 Aarhus C, Denmark

K. Schwarz
Institute of Technical Electrochemistry, Technical University of Vienna, Getreidemarkt 9, A-1060 Vienna, Austria
(Received 22 December 1980)

Angle-resolved-photoemission measurements have been performed on the (100) surface of a $TiN_{0.83}$ crystal. The bulk band structure of $TiN_{1.0}$ has been calculated using the linear augmented-plane-wave method, and the results are used to interpret the experimental data. The locations and dispersions of the bulk valence bands are mapped out along the $\Gamma \rightarrow X$ symmetry line and at various polar angles along the $\langle 011 \rangle$ azimuth. Emission from a surface-induced state located in a band gap at the Γ point in the surface Brillouin zone has been detected.

I. INTRODUCTION

The electronic structure of transition-metal nitrides and carbides has long been an intriguing question[1-3] because of the exceptional bonding properties these compounds exhibit. Many experimental[4-17] and theoretical[6,7,18-23] studies of the electronic structure have been made in order to understand and discriminate among different proposed binding mechanisms. The majority of studies have been made on carbides, while only a few experimental investigations have been reported[4,13,16] on nitrides. To date, most of the experimental studies have provided information about the total density of occupied states and thus have not allowed a very detailed comparison to calculated band structures. However, by utilizing the angle-resolved-photoemission technique combined with tunable synchrotron radiation, it was recently demonstrated[16] that for TiN, individual energy bands could be identified unambiguously and their dispersions mapped out, assuming direct transitions and a free-electron-like final state. Direct transitions were shown[16] to make a dominant contribution to the photoemission spectrum from a nonstoichiometric crystal, $TiN_{0.83}$. In a similar study[17] of $TiC_{0.93}$ crystals, the identification of individual bands and the mapping of their dispersions were found to be difficult because three-dimensional density-of-states features were observed in normal emission spectra at most photon energies. These features were attributed[17] to either the effects of bulk vacancies in the crystal or to surface inhomogeneities incurred in the process of preparing clean surfaces. For stoichiometric compounds, the applicability of the direct-transition model has been demonstrated,[24,25] but an indirect one-dimensional density-of-states model has also been used previously.[26,27] How well the direct-transition model works for interpreting the results from nonstoichiometric compounds, which are of great importance for a large class of materials, is thus still unresolved.

In the previous paper[16] on TiN, a free-electron-like final state was assumed. This assumption was made due to lack of band-structure data at the final-state energies involved. In this paper the results of linear augmented-plane-wave (LAPW) band-structure calculations for the stoichiometric composition $TiN_{1.0}$, carried out to final-state energies of about 35 eV above the Fermi level, are reported and used in the analysis of angle-resolved-photoemission results. Experimental data taken both at normal emission, using different photon energies, and as a function of electron emission angle

are presented and analyzed. The results, which represent a detailed study of the (100) surface, clearly demonstrate the applicability of the direct-transition model for the nonstoichiometric crystal studied, $TiN_{0.83}$.

II. EXPERIMENTAL

Experiments have been performed using both synchrotron radiation, from the 8° branch line at Stanford Synchrotron Radiation Laboratory (SSRL), and resonance radiation from a conventional uv lamp (He I and Ne I radiation; 21.2, and 16.85 eV, respectively). At SSRL, a Vacuum Generators ADES 400 photoemission system, which had an acceptance angle of $\pm 2°$, was utilized. When using resonance radiation, a spectrometer[28] equipped with a small movable hemispherical electrostatic analyzer was utilized, having an acceptance "cone" represented by a rectangle of dimensions $\pm 1°$ by $\pm 3°$. Both spectrometer systems were operated at an energy resolution of ≤ 0.20 eV and had base pressures of $< 1 \times 10^{-10}$ Torr.

The preparation and cleaning of the $TiN_{0.83}$ crystal has been described previously.[13] The cleanliness of the sample was checked using Auger electron spectroscopy, and no signals from residual contaminants, such as oxygen or sulfur, were detected after cleaning. In the ADES 400 system, the crystal was oriented azimuthally using low-energy electron diffraction (LEED). In the other spectrometer the crystal was oriented azimuthally, prior to mounting, with the aid of x-ray diffraction and the channeling pattern observed in a scanning electron microscope.

In the spectra shown below, the incidence angle of the radiation, θ_i, is given relative to the sample surface normal. The azimuthal angle ϕ is given as the direction parallel to the electric field vector of linearly polarized radiation (in the horizontal plane) for normal incidence, i.e., at $\theta_i = 0°$. In both spectrometers, the analyzers were movable in the horizontal plane. The radiation from the uv lamp was unpolarized. The midpoint of the Fermi edge is used as the reference level for all spectra.

III. RESULTS AND DISCUSSION

A. Band-structure calculation

In order to represent the final state by band energies, the bands are needed up to about 35 eV above E_F. For the present analysis these energies are calculated for the plane through the Brillouin zone, which is surrounded by the k points $\Gamma-(\Delta)-X-U-L-K-(\Sigma)-\Gamma$. In this plane, a uniform mesh of 149 k points is obtained when the Δ direction is divided into 16 and the Σ into 12 intervals.

Since none of the available band structures for TiN provide such data, i.e., band energies on a fine k grid and up to sufficiently high energies, new calculations have been performed in two steps: First, the band-structure calculation by Neckel *et al.*[22] was extended to higher energies, but only for a few selected k points. This calculation employed the augmented-plane-wave (APW) method and made full use of symmetry. In the second part the linearized version of the APW method (LAPW),[29,30] without symmetry, was used to obtain the band energies on the relatively fine k mesh, since this method is significantly faster than the APW program. The linearization in the LAPW scheme yields accurate bands over an energy range of about 1 Ry. Therefore four energy regions were used to span the whole energy range of interest. The following parameters, E_l (for definitions, see Ref. 30), for the radial wave functions inside the atomic spheres were chosen:

region 1: N sphere $E_l = 0.4$ Ry except $E_s^{\mathrm{N}} = 0.4$ Ry,

Ti sphere $E_l = 0.8$ Ry except $E_p^{\mathrm{Ti}} = 0.0$ Ry,

region 2: all $E_l = 1.6$ Ry,

region 3: all $E_l = 2.4$ Ry,

region 4: all $E_l = 3.2$ Ry except $E_d^{\mathrm{Ti}} = 2.8$ Ry .

With these parameters, the band energies from both the LAPW and APW methods agree to within a few mRy. By combining the LAPW results of the four energy sheets, we obtained the complete band structure illustrated in Fig. 1. Also included in Fig. 1 is the free-electron-like final state (dotted line) used in a previous[16] interpretation of photoemission data.

B. Normal-emission data

Two electron energy distribution curves (EDC's) recorded at normal electron emission with linearly polarized 21-eV radiation incident at $\theta_i = 15°$ and 75°, respectively, are shown in Fig. 2. A strong polarization effect is observed, which allows direct identification of the symmetry of the initial states.

For normal electron emission, symmetry selection rules[31] give that $E_{\parallel}$, i.e., the component of the electric field parallel to the surface, excites only initial states of Δ_5 symmetry while $E_{\perp}$, i.e., the electric

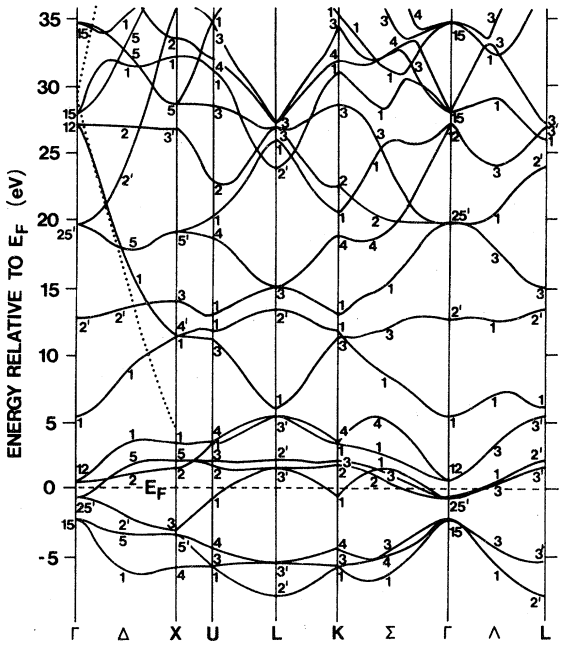

FIG. 1. Energy bands of $TiN_{1.0}$ obtained by the LAPW method. The free-electron-like final state assumed in a previous analysis (Ref. 16) of photoemission data is also shown (dotted line).

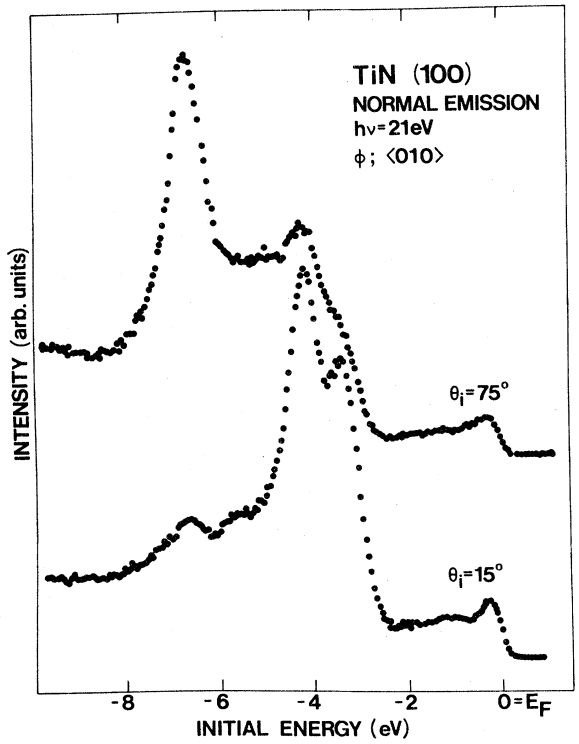

FIG. 2. Angle-resolved EDC's for normal electron emission from TiN(100) for 21-eV photons incident at 15° and 75° relative to the sample surface normal.

field component along the surface normal, excites only initial states of Δ_1 symmetry. Even without consideration of reflection and refraction at the TiN surface, it should be true, in general, that $E_{\|}/E_{\perp}$ will be larger for $\theta_i = 15°$ than for $\theta_i = 75°$ at a given photon energy. The peak around -6.5 eV is most clearly observed in the spectrum recorded at $\theta_i = 75°$ and can thus unambiguously be associated with emission from a Δ_1 initial-state band. The doublet between about -3 and -5 eV, which is most pronounced in the spectrum recorded at $\theta_i = 15°$, can likewise be identified as arising from Δ_5 initial states.

The evolution of the EDC's with photon energy is shown in Figs. 3(a) and 3(b) for $\theta_i = 15°$ and 75°, respectively. Concentrating first on the spectra shown in Fig. 3(a), we clearly observe dispersion of the main structure, located between about -3 and -5 eV, which previously was assigned to Δ_5 initial states. Dispersion is also observed for the weak peak, located at about -2 eV in the 13-eV spectrum, which is seen to move towards the Fermi level with increasing photon energy. These observations are taken as evidence of direct transitions. If indirect transitions made the dominant contribution, the spectra would reflect the one-dimensional density of states[26,27] and no dispersion of peaks with photon energy should be observed. Dispersion is also observed in the spectra of Fig. 3(b).

In a previous report[16] a free-electron-like final-state band was assumed when mapping the band dispersions along the $\Gamma \rightarrow X$ symmetry line using the direct-transition model. Here we instead use the calculated LAPW band structure and the condition that only Δ_1 final-state bands contribute at normal electron emission.[31] The calculated band structure of $TiN_{1.0}$ along the $\Gamma \rightarrow X$ symmetry line is shown in Fig. 4 together with our experimental results. The solid dots represent data for initial-state bands that could be unambiguously identified. The dotted lines represent the position of shoulders while the open dots represent peaks observed in the spectra that could not be unambiguously identified. The vertical bars indicate the estimated uncertainty in the determination of peak positions for the cases where it is larger than 0.1 eV.

A comparison between the data given as solid dots in Fig. 4 and the calculated bands yields the following: Both the Δ_5 and Δ_1 bands are located closer to the Fermi level in the calculation than what is obtained experimentally. Our data locate the Γ_{15} point at $-3.4(\pm 0.1)$ eV, the X_5' point at $-4.0(\pm 0.2)$ eV, and the X_4' point at $-6.4(\pm 0.2)$ eV

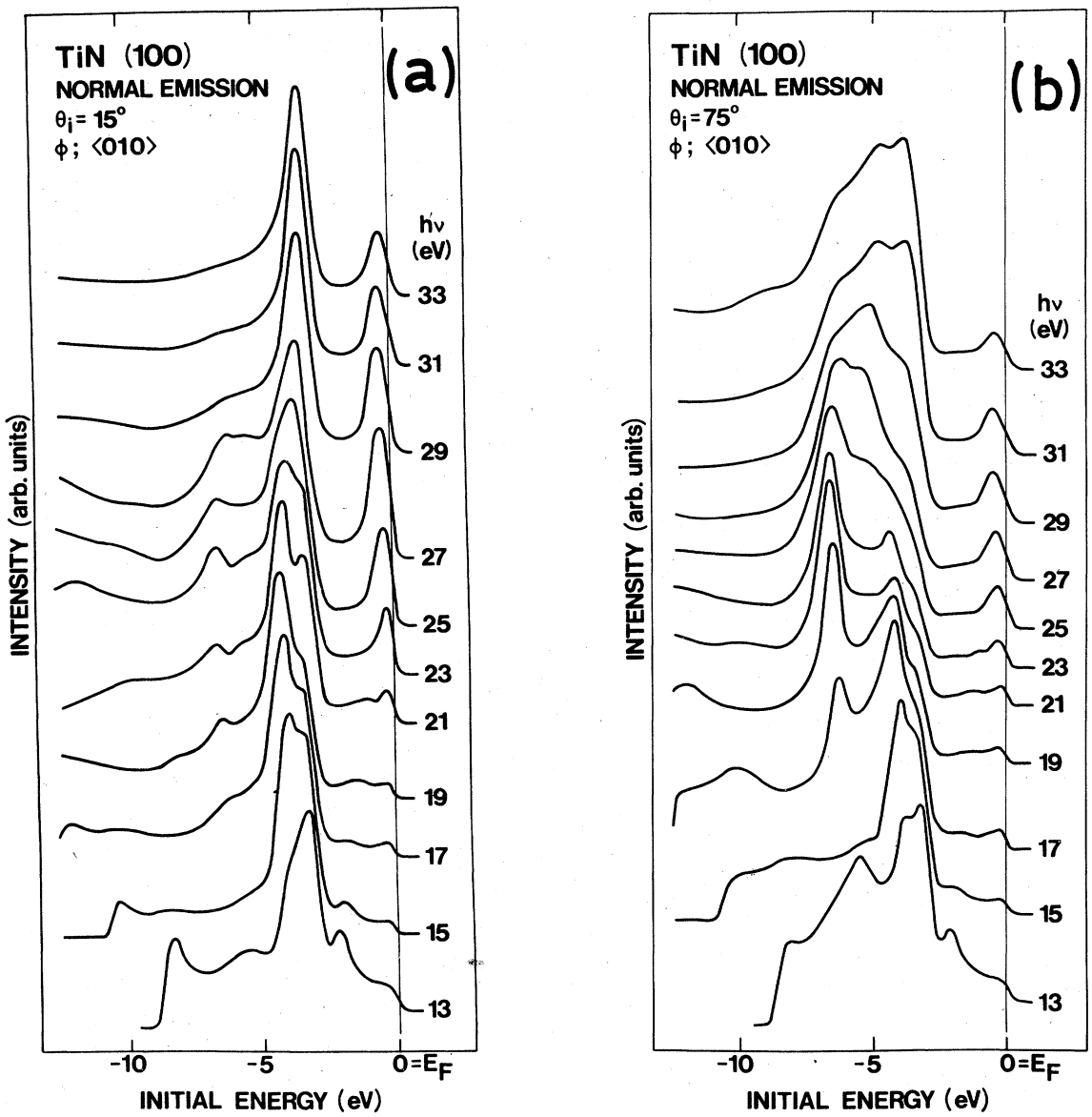

FIG. 3. Angle-resolved EDC's for normal electron emission from TiN(100) for different photon energies. The incidence angle of the radiation is (a) $\theta_i = 15°$ and (b) $\theta_i = 75°$.

versus -2.2, -3.3, and -5.9 eV, respectively. The dispersion of the Δ_5 band is mapped out along the entire $\Gamma \rightarrow X$ line while only the flattest part of the Δ_1 band is mapped out. The dispersion of the Δ_2' band is also mapped out along part of the $\Gamma \rightarrow X$ line and, in this case, the experimental points are closer to the Fermi level than the calculated band. Our data locate the X_3 point at $-2.3(\pm 0.3)$ eV instead of at -3.2 eV. It should be noted that symmetry selection rules[31] forbid observation of the Δ_2' band at normal electron emission. However, this applies strictly only for a system with a vanishingly small acceptance solid angle. The acceptance angle of $\pm 2°$ in the ADES 400 system therefore permits electrons excited from the Δ_2' band, although strictly forbidden in normal emission, to be observed.

Upon a closer examination of the spectra shown in Fig. 3, two additional observations are made. First, an increase in the intensity of the peak just below the Fermi level is observed at photon energies between 23 and 31 eV [see Fig. 3(a)]. The explanation is that at these energies, the uppermost Δ_5 band (seen in Fig. 4) contributes to the emission. Secondly, some weak and broad features are ob-

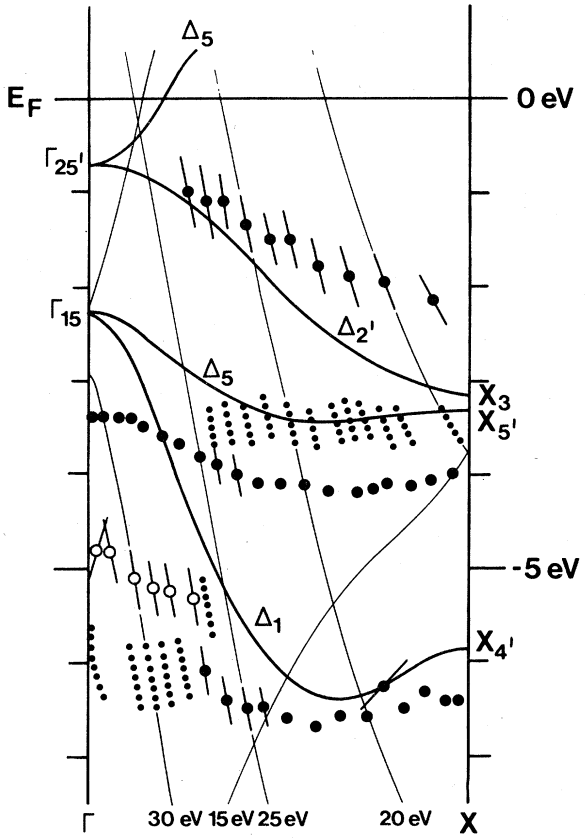

FIG. 4. Calculated and experimental energy band dispersions along the ⟨100⟩ direction for TiN. The light solid lines represent the Δ_1 final-state bands displaced downwards by the amount indicated. See text for details.

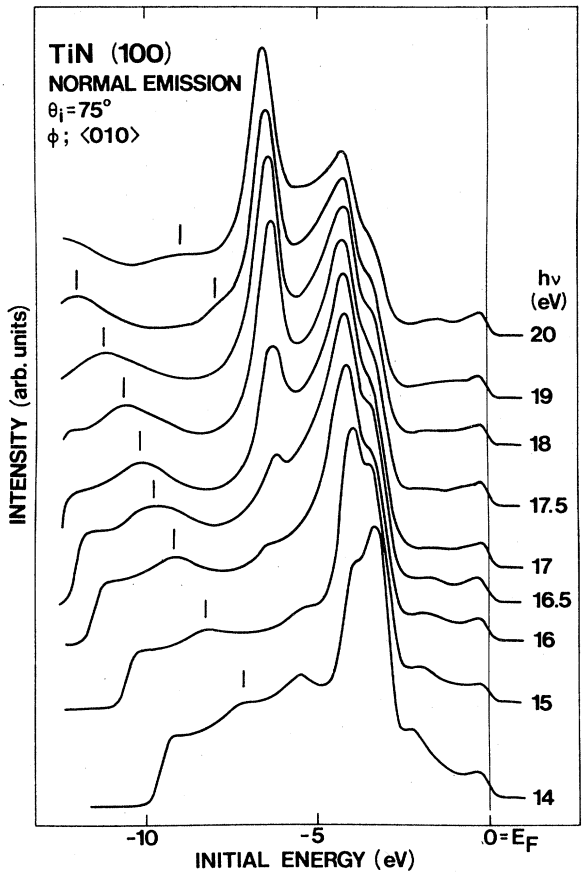

FIG. 5. Normal emission spectra for TiN(100) measured at various photon energies for $\theta_i = 75°$. The two final-state features observed in the spectra are indicated by hatch marks.

served below the main structures in some of the spectra. These features are interpreted as final-state effects which are further illustrated in Fig. 5. Two final-state features are observed in Fig. 5 (and also in Fig. 3). If these features are interpreted as arising from a high density of final states at the critical points Γ_1 and X_1 (X_4') (see Fig. 1), we obtain experimental values of 6.7(±0.5) eV and 11(±1) eV, respectively, while the calculated locations are 5.3 and 11.3 eV. Possible origins of the peaks and shoulders shown as open dots and dotted lines in Fig. 4 are discussed below.

C. Polar-angle dependence

In order to perform a further mapping of the bulk band structure, measurements were also made as a function of electron emission angle. EDC's recorded at different polar angles, θ_e, along the ⟨011⟩ azimuth, using unpolarized He I (21.2 eV) radiation, are shown in Fig. 6. For the spectra shown in Fig. 6(a), the incidence angle θ_i is 15°, while it is 45° for those shown in Fig. 6(b). Care was taken in these measurements to better resolve the previously observed doublet arising from Δ_5 initial states at normal emission (see Figs. 2 and 3). Two well-resolved peaks, labeled *B* and *C*, are also clearly observed at $\theta_e = 0°$ in Fig. 6. The energy positions of these two peaks are seen to vary quite strongly as a function of polar angle. The position of the peak around −6.5 eV (labeled *D* and arising from Δ_1 initial states at normal emission) exhibits a weak variation with θ_e, however. The peak labeled *A* in Fig. 6 corresponds to the structure arising from Δ_2' initial states at normal emission.

The energy positions of peaks *A*, *B*, *C*, and *D* are plotted versus polar angle in Fig. 7. The vertical bars on the data points indicate the estimated uncertainty of peak positions for cases where it is larger than ±0.1 eV. Also shown in Fig. 7 are the cal-

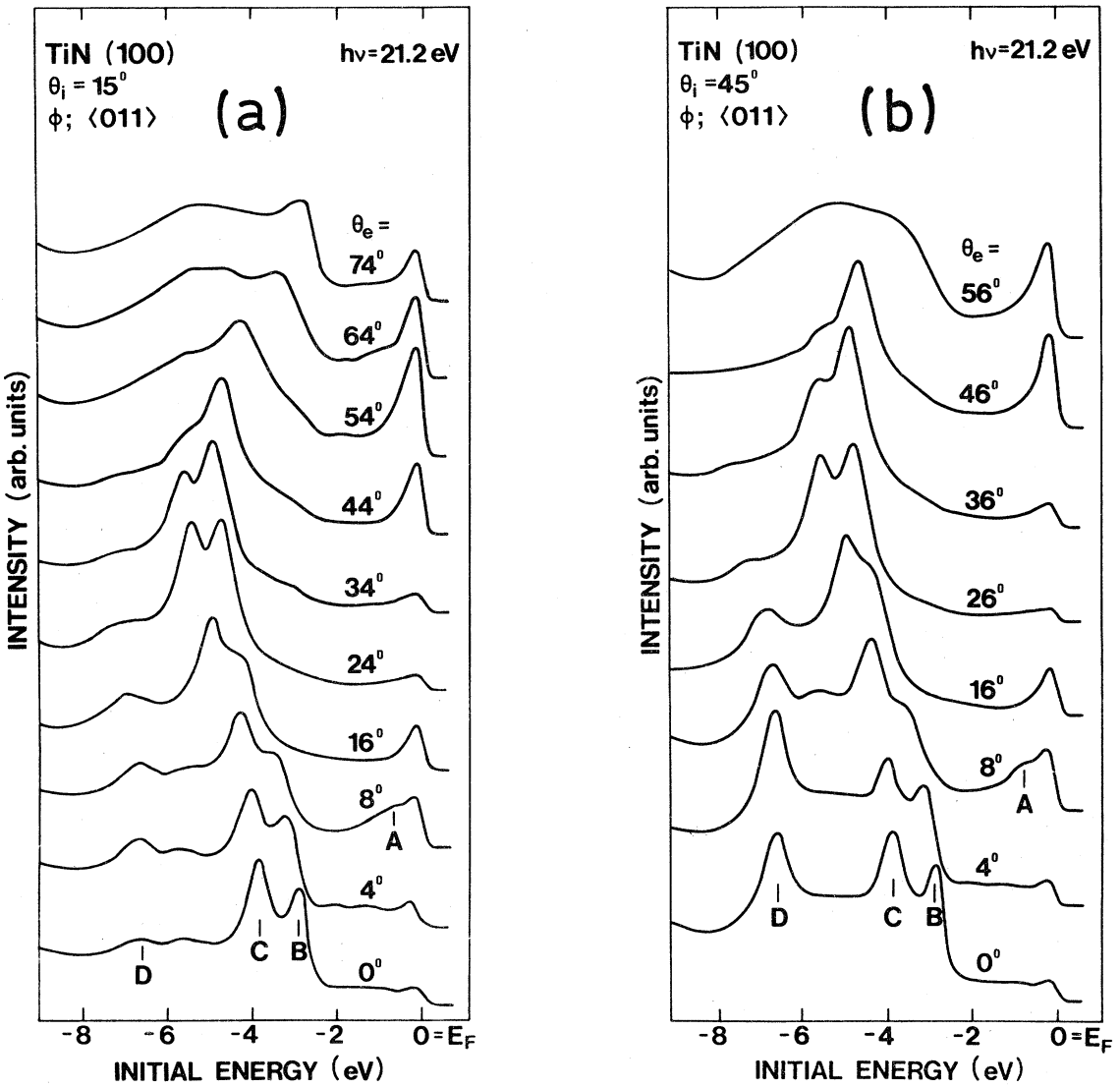

FIG. 6. Angle-resolved EDC's from TiN(100) measured at various polar angles, θ_e, using unpolarized HeI radiation. In (a) $\theta_i = 15°$ and in (b) $\theta_i = 45°$.

culated energy positions. The dashed curves are obtained using the full calculated band structure, while the dotted curves use the free-electron-like final-state band illustrated in Fig. 1. Initial-state surfaces, on which direct transitions between bands are possible, were calculated[32] in the repeated zone scheme of $\vec{k}$ space. An interpolation of the calculated band structure on a denser mesh in $\vec{k}$ space was performed in this calculation. The final-state energy and momentum is known at each point on these surfaces. By assuming conservation of $k_{||}$ (the momentum component parallel to the surface) during propagation through the surface the detection angle for electrons which have undergone direct transitions becomes

$$\theta_e = \arcsin \frac{\hbar |k_{||}|}{|2m(E_i - E_F + h\nu - \phi)|^{1/2}} ,$$

where $E_i - E_F$ represents the initial-state energy, relative to the Fermi level, and ϕ is the work function. A work-function value of 4.0 eV has been used[33] for the calculated curves shown in Fig. 7. The calculated contributions to the emission were separated into primary and secondary cones.[34] Primary-cone emission makes the dominant contribution up to emission angles of about 45°. For larger emission angles,

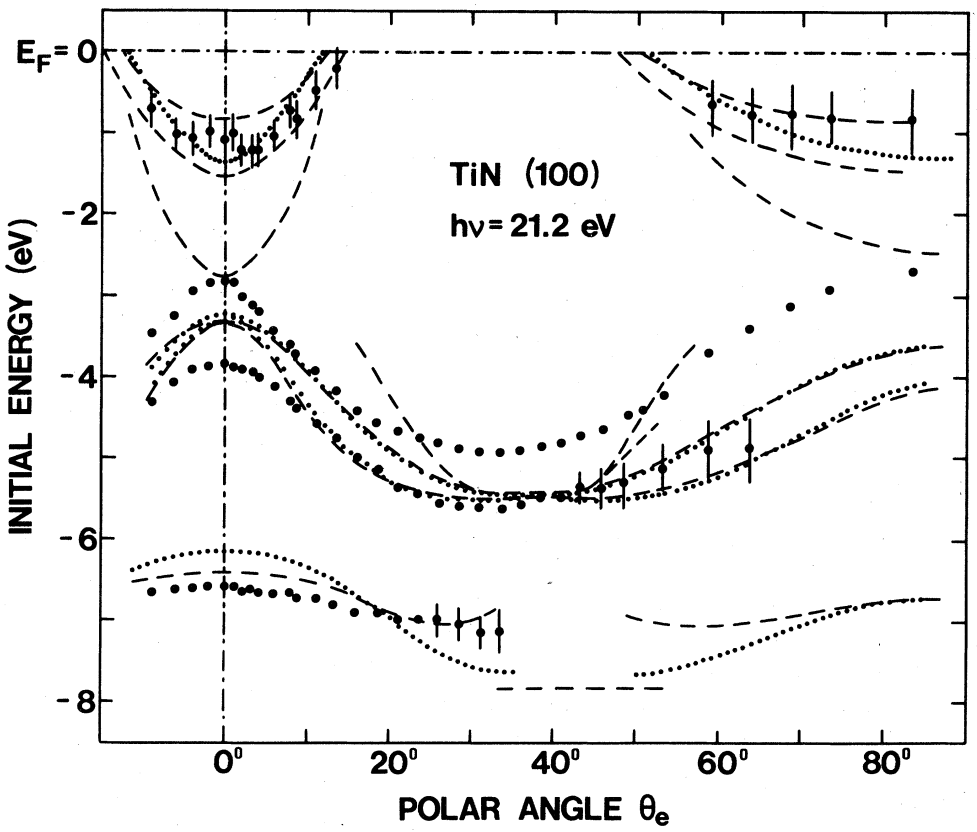

FIG. 7. Comparison between experimental and calculated peak positions as functions of polar angle along the ⟨011⟩ azimuth. See text for details.

secondary-cone emission, involving $G_{1\bar{1}\bar{1}}$ and $G_{\bar{1}\bar{1}\bar{1}}$ reciprocal-lattice vectors, accounts for the emission. We notice that the final-state band dispersion is very free-electron-like at this energy. The dashed curves (full calculated band structure) follow fairly closely the dotted curves (free-electron-like final state) in Fig. 7, apart from some branches of the dashed curves that originate from final-state bands which the single free-electron-like final-state band cannot reproduce.

The trends in the experimental polar-angle dependence of peak positions agree well with the trends of the calculated curves. We concentrate on the dashed curves (full calculated band structure) in the comparison. The agreement in peak positions is as good as one could expect to achieve, judging from the normal emission data. Peaks C and D lie deeper below E_F than the calculated values by 0.8 and 0.2 eV, respectively, at $\theta_e = 0°$. Peak A, however, lies about 0.2 eV closer to E_F than the calculated position at $\theta_e = 0°$, but the angle dependence agrees satisfactorily with the calculated dependence.

There are branches of the calculated curves for which we do not observe any corresponding features in the recorded spectra. Close to E_F and at small emission angles there are two such branches and between emission angles of 20° and 60° there are two other such branches at initial-state energies between -3 and -5 eV. The calculated curves show three branches close to E_F at emission angles larger than about 50°, among which we cannot discriminate. However, a careful examination of the recorded spectra reveals an intensity increase of the peak just below E_F at angles around 50°. And, for larger emission angles, a weak structure appears below this peak. The determined positions of this weak structure are also given in Fig. 7.

The most intriguing discrepancy between experimental and calculated results occurs for peak B in Fig. 6, which we believe has no counterpart in the calculated curves. This peak was observed also in the normal emission spectra (see Figs. 2 and 3). The origin of this peak will be discussed in a later section.

In Fig. 8, EDC's reorded at different polar angles, along the ⟨011⟩ azimuth, using unpolarized

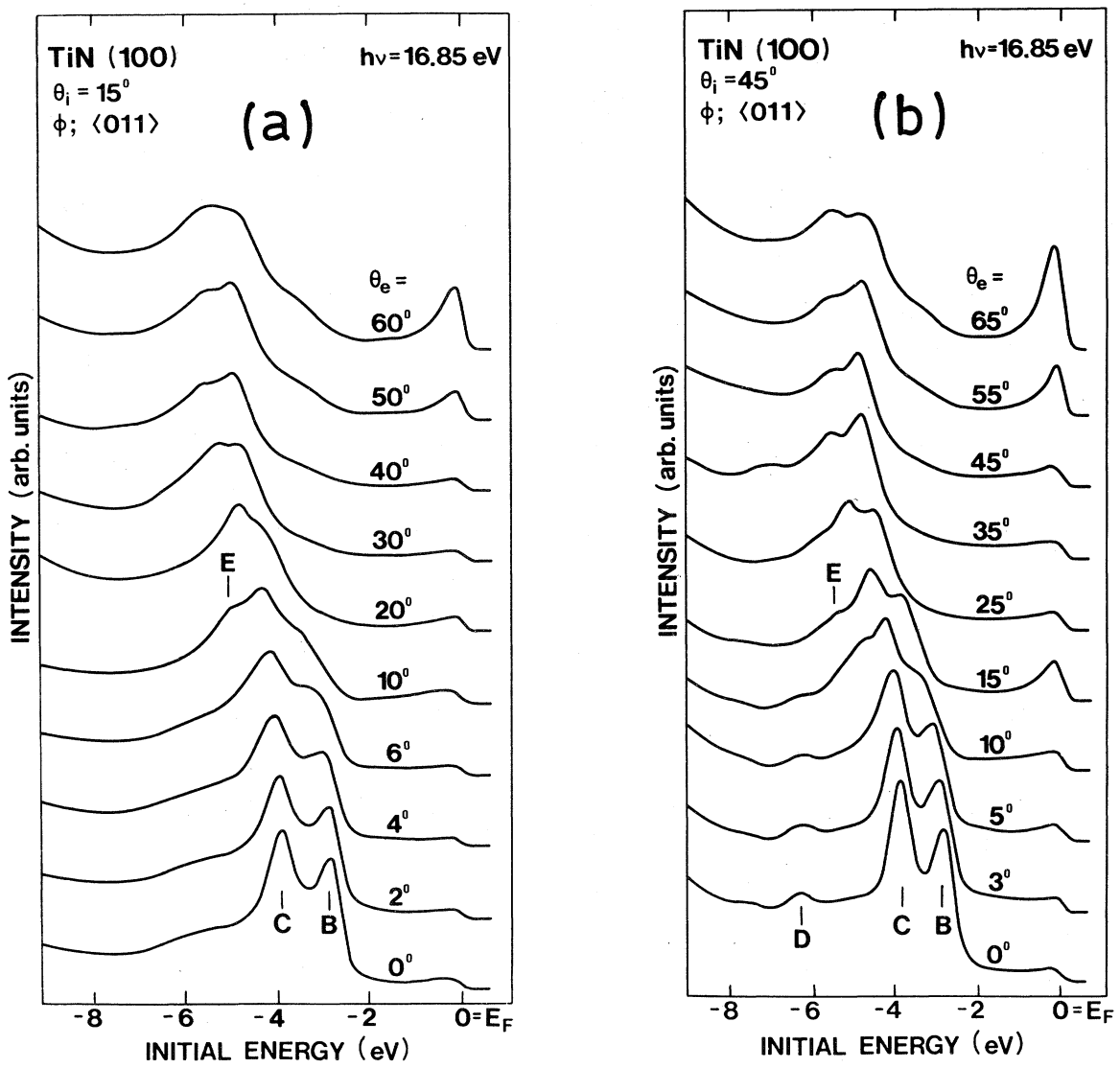

FIG. 8. Angle-resolved EDC's from TiN(100) measured at various polar angles, θ_e, using unpolarized Ne I radiation. In (a) $\theta_i = 15°$ and in (b) $\theta_i = 45°$.

Ne I radiation, are shown. The incidence angle θ_I is 15° and 45° for the spectra shown in Figs. 8(a) and 8(b), respectively. Three peaks, labeled *B*, *C*, and *D*, are clearly seen in these spectra. At polar angles between about 10° and 20°, a shoulder *E* appears. No peak corresponding to the peak labeled *A* in Fig. 6 is observed at polar angles of less than 10°. The energy positions of peaks *B*, *C*, *D*, and *E* are plotted versus polar angle in Fig. 9.

Also shown in this figure are the calculated curves, where the dashed and dotted curves represent results obtained using the full calculated band structure and the free-electron-like final-state band, respectively. Also at this photon energy the final state is seen to be rather free-electron-like. The angle dependence of the dotted curves closely follows branches of the dashed curves. For the deepest-lying band and the band closest to E_F the two calculations differ by about 0.5 eV at small polar angles. There is only one branch of the dashed curves that has no counterpart in the dotted curves. That branch originates from the final-state band which, along $\Gamma \rightarrow X$, has the symmetry Δ_2' (see Fig. 1).

Also at this photon energy the trends in the experimental polar-angle dependence of peak positions

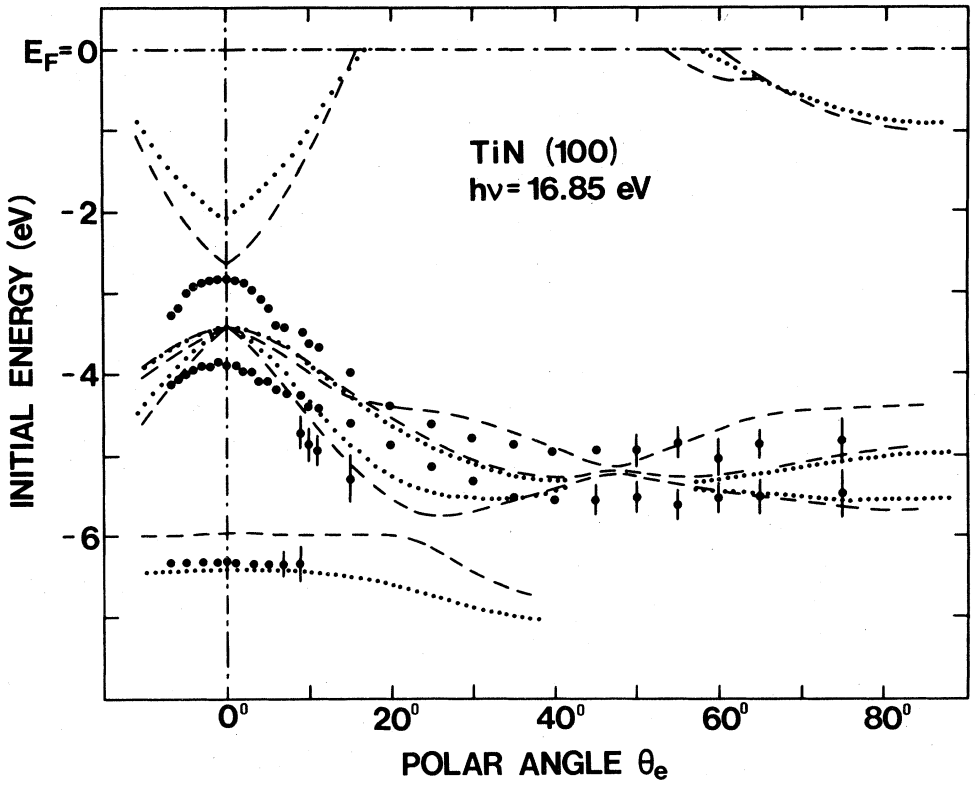

FIG. 9. Comparison between experimental and calculated peak positions as functions of polar angle along the ⟨011⟩ azimuth. See text for details.

agree well with the trends of the calculated curves. However, around $\theta_e = 0°$, peaks C and D lie about an additional 0.4 eV below E_F than the calculated values (dashed curves). No distinct peak corresponding to the branches of the calculated curves closest to E_F was observed. The increased intensity of the structure just below E_F at polar angles around 15° and greater than about 50° may, however, be interpreted as arising from the onset of these branches.

D. Discussion

Most of the structures observed in the photoemission spectra from the (100) surface of the $TiN_{0.83}$ crystal studied can be explained in terms of direct transitions between calculated bulk bands. There are, however, some features observed that we have not yet tried to explain.

In the normal emission spectra recorded at $\theta_i = 75°$ and at photon energies > 27 eV, structures appear that cannot be explained by direct transitions to a Δ_1 final state [see Fig. 3(b)]. The locations of these peaks and shoulders, at initial-state energies between -4.5 and -6.5 eV, are shown as open dots and dotted lines in Fig. 4. The origin of these features is uncertain but they arise either from a more complicated final state or from density-of-state effects.[35] At these photon energies, there are actually other final states available, as seen in Fig. 1. When the experimental geometry favors the observation of emission from Δ_5 initial states these extra features are not observed [see Fig. 3(b)]. However, the presence of bulk vacancies, which give rise to compositional disorder, may affect[36] the conservation relations governing the direct photoemission process. Thus, although direct transitions clearly make the dominant contribution in most of the spectra shown, we can not rule out density-of-states effects as the origin of these features observed at high photon energies.

At photon energies of < 24 eV, a peak is observed in the normal emission spectra around -3.4 eV that cannot be accounted for using the calculated bulk band structure of $TiN_{1.0}$ and the direct-transition model. The polarization dependence of

this peak (see Fig. 2) indicates that along the $\Gamma \rightarrow X$ line it arises from an initial state of Δ_5 symmetry. This peak is located more than half an eV closer to the Fermi level that the peak interpreted as arising from the bulk band of Δ_5 symmetry. The mapping of the dispersions of these two peaks (Fig. 4) suggests that there is an extra band of Δ_5 symmetry along the $\Gamma \rightarrow X$ line compared to the predictions of the calculated bulk band structure. The polar-angle dependence of the positions of these two peaks also supports the presence of an extra band. The peaks, labeled *B* and *C* in Figs. 6 and 8, exhibit very similar dependencies with polar angle, as seen in Figs. 7 and 9. Interpreting peak *C* as arising from bulk band transitions leaves peak *B* unaccounted for. The energy separation between these peaks, determined from the HeI and NeI spectra at $\theta_e = 0°$, is $1.0(\pm 0.2)$ eV. What effects might explain the presence of an extra energy band?

Spin-orbit interactions, if included in the band-structure calculation, would cause a splitting of the degenerate Δ_5 band at X_5' (see Fig. 4). The observed splitting, > 0.5 eV close to X_5', seems to be too large to be explained by spin-orbit interactions, however. In measurements on Cu, for example, a spin-orbit splitting of the X_5 level of 0.1 eV has been observed.[37]

The question should be raised whether bulk vacancies could give rise to extra bands, compared to the bulk band structure at stoichiometric compositions. In a similar case, namely that of VC_x, two calculations have been reported[38,39] which studied the effects of carbon vacancies by means of the simple virtual crystal approximation. The band structure for VC_x, with x varying between 0.7 and 1.0, looked very much the same, except for small shifts in band positions. Recently, a more advanced method using the coherent potential approximation was used to calculate the density of states of substoichiometric TiC_x (Ref. 40) and TiN_x (Ref. 41). In all these cases, it was concluded that no extra bands originated from vacancy states. Although both types of calculations employed approximations, these results indicate that it is unlikely that the observed band should originate from effects of nonstoichiometry.

Can it be a surface-induced state? In order to classify a peak in a photoemission spectrum as arising from a surface-induced state the following requirements need to be fullfilled. Its position should be insensitive to variations of photon energy[42] because it is a two-dimensional state and should not exhibit any dispersion with $k_\perp$, the momentum component perpendicular to the surface. Surface states are commonly considered to be sensitive to surface contamination.[42] Furthermore, surface-induced states are trapped in band gaps[43] of the bulk band structure. In Fig. 4, we see that the first requirement is fullfilled. The position of the peak (shoulder) is $-3.4(\pm 0.3)$ eV, independent of photon energy. It should be noted that in the spectra shown in Figs. 6 and 8, the position of peak *B* is $-2.9(\pm 0.1)$ eV for $\theta_e = 0°$. This latter value is considered a better determination, since the peak associated with surface-state emission is much better resolved in these spectra. The peak is also found to be sensitive to surface contamination. At CO exposures of ≤ 1 langmuir ($1\ \text{L} = 10^{-6}$ Torr sec) this peak is strongly attenuated, while the peaks associated with bulk band emission are very little affected.[44] What about the third requirement. Does the state fit into a gap of the bulk band structure? The calculated band structure shows no energy gaps when projected along Δ ($\Gamma - X$ line) onto the Γ point in the surface Brillouin zone (SBZ). Our experimental results, however (which are summarized in Table I), locate the bands differently. When the bulk bands are projected onto Γ in the SBZ, using the locations of the critical points X_3, X_5', and Γ_{15} extracted from the experimental data, indeed, a band gap appears between about -2.3 and -3.4 eV. The observed state fits nicely into this gap. Based on the above arguments, we conclude that a surface-induced state is observed between the third and fourth bulk bands (counting from below in Fig. 1 and taking into account that the Δ_5 band is degenerate).

IV. SUMMARY

Using the technique of angle-resolved photoemission, we have mapped the locations and dispersions of the energy bands for a TiN(100) crystal. The

TABLE I. Critical-point energies, relative to E_F, for TiN.

Point	Expt.	Calc.	Neckel *et al.* (Ref. 22)	Ern *et al.* (Ref. 18)
Γ_1	6.7 ± 0.5	5.3	5.6	5.7
Γ_{15}	-3.4 ± 0.1	-2.2	-2.0	-1.7
$X_1(X_4')$	11 ± 1	11.3	11.5	
X_3	-2.3 ± 0.3	-3.2	-3.0	-2.4
X_5'	-4.2 ± 0.2	-3.3	-3.1	-2.6
X_4'	-6.4 ± 0.2	-5.9	-5.7	-4.9

direct-transition model was shown to account for most of the structures observed in the spectra from the nonstoichiometric crystal studied, $TiN_{0.83}$. The band structure of $TiN_{1.0}$ was calculated using the LAPW method and the results were used in the analysis of the experimental data. The overall agreement between calculated and experimental results is very encouraging, considering this is the first detailed bandmapping performed on TiN. The band dispersions are reproduced fairly well by the experimental results, but the actual band positions differ by up to about 1.5 eV, as summarized in Table I.

A peak observed in the photoemission spectrum was attributed to emission from a surface-induced state, using the commonly applied criteria. The experimentally determined bulk bands yield a band gap, into which the observed state fits nicely when projected along Δ onto the Γ point in the SBZ.

The applicability demonstrated for the direct-transition model on a crystal containing a fair amount of vacancies, and thus having compositional disorder, should be of importance for a large class of materials.

ACKNOWLEDGMENTS

The authors thank M. L. Shek for experimental help and Dr. G. O. Arbman for providing an LAPW program which was adapted for the present calculation. The band-structure computations were performed at "Interfakultäres Rechenzentrum der Technischen Universität Wien." Part of the experiments were performed at the Stanford Synchrotron Radiation Laboratory, which is supported by the National Science Foundation under Contract No. DMR 77-27489 in cooperation with the Stanford Linear Accelerator Center and the Department of Energy.

[1]E. K. Storms, *The Refractory Carbides* (Academic, New York, 1967).
[2]L. E. Toth, *Transition Metal Carbides and Nitrides* (Academic, New York, 1971).
[3]W. S. Williams, Prog. Solid State Chem. 6, 57 (1971).
[4]L. Ramqvist, K. Hamrin, G. Johansson, A. Fahlman, and C. Nordling, J. Phys. Chem. Solids 30, 1835 (1969); 31, 2669 (1970).
[5]D. W. Fischer, J. Appl. Phys. 41, 3922 (1970).
[6]H. Ihara, Y. Kumashiro, and A. Itoh, Phys. Rev. B 12, 5465 (1975); 14, 1707 (1976).
[7]J. F. Alward, C. Y. Fong, M. El-Batanouny, and F. Wooten, Phys. Rev. B 12, 1105 (1975); Solid State Commun. 17, 1063 (1975).
[8]V. A. Gubanov and E. Z. Kurmaev, Int. J. Quantum Chem. 9, 297 (1975).
[9]K. Schwarz, A. Neckel, and A. M. Bradshaw, Chem. Phys. Lett. 41, 311 (1976).
[10]S. Manninen and T. Paakkari, J. Phys. C 9, 95 (1976).
[11]L. I. Johansson, A. L. Hagström, B. E. Jacobson, and S. B. M. Hagström, J. Electron Spectrosc. Relat. Phenom. 10, 259 (1977).
[12]A. L. Hagström L. I. Johansson, S. B. M. Hagström, and A. N. Christensen, J. Electron Spectrosc. Relat. Phenom. 11, 75 (1977).
[13]L. I. Johansson, P. M. Stefan, M. L. Shek, and A. N. Christensen, Phys. Rev. B. 22, 1032 (1980).
[14]J. H. Weaver and F. A. Schmidt, Phys. Lett. 77A, 73 (1980).
[15]A. M. Bradshaw, J. F. van der Veen, F. J. Himpsel, and D. E. Eastman, Solid State Commun. 37, 37 (1980).
[16]L. I. Johansson, P. M. Stefan, M. L. Shek, and A. N. Christensen, Solid State Commun. 36, 965 (1980).
[17]J. H. Weaver, A. M. Bradshaw, J. F. van der Veen, F. J. Himpsel, D. E. Eastman, and C. Politis, Phys. Rev. B 22, 4921 (1980).
[18]V. Ern and A. C. Switendick, Phys. Rev. A 137, 1927 (1965).
[19]J. B. Conklin, Jr. and D. J. Silversmith, Int. J. Quantum Chem. IIS, 243 (1968).
[20]D. J. Chadi and M. L. Cohen, Phys. Rev. B 10, 496 (1974).
[21]H. R. Trebin and H. Bross, J. Phys. C 8, 1181 (1975).
[22]A. Neckel, P. Rastl, R. Eibler, P. Weinberger, and K. Schwarz, J. Phys. C 9, 579 (1976).
[23]V. A. Gubanov, A. L. Ivanovskii, G. P. Shveikin, and J. Weber, Solid State Commun. 29, 743 (1979).
[24]T. C. Chiang, J. A. Knapp, M. Aono, and D. E. Eastman, Bull. Am. Phys. Soc. 24, 366 (1979).
[25]M. Aono, T. C. Chiang, J. A. Knapp, T. Tanaka, and D. E. Eastman, Solid State Commun. 32, 271 (1979).
[26]T. Grandke, L. Ley, and M. Cardona, Phys. Rev. Lett. 38, 1033 (1977).
[27]P. Thiry, P. Pinchaux, G. Martinez, Y. Petroff, J. Lecante, J. Paigne, Y. Ballu, C. Guilliot, and D. Spanjaard, Solid State Commun. 27, 99 (1978),
[28]I. Lindau and S. B. M. Hagström, J. Phys. E 4, 936 (1971).
[29]O. K. Andersen, Phys. Rev. B 12, 3060 (1975).
[30]D. D. Koelling and G. O. Arbman, J. Phys. F 5, 2041 (1975).
[31]J. Hermanson, Solid State Commun. 22, 9 (1977).
[32]The computer program used was developed by G. V. Hansson and S. Person. See G. V. Hanson, Linköping Studies in Science and Technology, Dissertation No. 23, 1978 (unpublished).
[33]M. A. Eremaev *et al.*, Zh. Tekh. Fiz. 44, 2159 (1974) [Sov. Phys. Techn. Phys. 19, 1337 (1975)] report measured work-function values between 3.7 and 4.0 eV for TiN.
[34]G. D. Mahan, Phys. Rev. B 2, 4334 (1970).
[35]Density-of-states effects are discussed in Ref. 17.
[36]N. J. Shevchik, Phys. Rev. B 16, 3428 (1977).

[37]This value is quoted by P. Heimann, J. Hermanson, H. Miosga, and H. Neddermeyer, Phys. Rev. B 20, 3059 (1979).
[38]J. Zbasnik and L. E. Toth, Phys. Rev. B 8, 452 (1973).
[39]A. Neckel, P. Rastl, K. Schwarz, and R. Eibler-Mechtler, Z. Naturforsch. 29a, 107 (1974).
[40]J. Klima, J. Phys. C 12, 3691 (1979).
[41]J. Klima, Czech. J. Phys. B 30, 905 (1980).
[42]M. Kawajiri, J. Hermanson, and W. Schwalm, Solid State Commun. 25, 303 (1978).
[43]J. B. Pendry and S. J. Gurman, Surf. Sci. 49, 87 (1975).
[44]The sensitivity of the TiN(100) surface to different adsorbates will be discussed in a forthcoming publication.